Lead-iodide nanowire perovskite with methylviologen showing interfacial charge-transfer absorption: A DFT analysis

ARTICLE *in* PHYSICAL CHEMISTRY CHEMICAL PHYSICS · JULY 2014

Impact Factor: 4.49 · DOI: 10.1039/c4cp01553c · Source: PubMed

2 AUTHORS:

Jun-Ichi Fujisawa
Gunma University
48 PUBLICATIONS **877** CITATIONS
SEE PROFILE

Giacomo Giorgi
The University of Tokyo
63 PUBLICATIONS **409** CITATIONS
SEE PROFILE

PCCP

PAPER

Cite this: *Phys. Chem. Chem. Phys.*, 2014, **16**, 17955

Lead-iodide nanowire perovskite with methylviologen showing interfacial charge-transfer absorption: a DFT analysis

Jun-ichi Fujisawa*[ab] and Giacomo Giorgi[c]

Received 10th April 2014,
Accepted 7th July 2014

DOI: 10.1039/c4cp01553c

www.rsc.org/pccp

Methylviologen lead-iodide perovskite ($MVPb_2I_6$) is a self-assembled one-dimensional (1-D) material consisting of lead-iodide nanowires and intervening organic electron-accepting molecules, methylviologen (MV^{2+}). $MVPb_2I_6$ characteristically shows optical interfacial charge-transfer (ICT) transitions from the lead-iodide nanowire to MV^{2+} in the visible region and unique ambipolar photoconductivity, in which electrons are transported through the three-dimensional (3-D) organic network and holes along the 1-D lead-iodide nanowire. In this work, we theoretically study the electronic band-structure and photocarrier properties of $MVPb_2I_6$ by density functional theory (DFT) calculations. Our results clearly confirm the experimentally reported type-II band alignment, whose valence band mainly consists of 5p (I) orbitals of the lead-iodide nanowires and the conduction band of the lowest unoccupied molecular orbital of MV^{2+}. The DFT calculation also reveals weak charge-transfer interactions between the lead-iodide nanowires and MV^{2+}. In addition, the electronic distributions of the valence and conduction bands indicate the 3-D transport of electrons and 1-D transport of holes, supporting the reported experimental result.

Introduction

Organic–inorganic metal–halide perovskites are self-assembled hybrid materials, which consist of anionic metal–halide semiconductive frameworks and charge-compensating organic cations.[1–3] For the organic–inorganic hybrid perovskites, the dimensionality of the inorganic framework can be controlled by the type of organic cations from 0 (dot) to 1 (wire), 2 (well) and 3 (bulk).[1–3] The optical and conductive properties of these perovskites have been studied extensively.[1–3] The photoconductive properties of the perovskites were first reported in 2005 for one-dimensional (1-D) lead-iodide nanowire perovskite ($MVPb_2I_6$) with methylviologen (MV^{2+}).[4] In 2009, Miyasaka's group developed TiO_2-based electrochemical photovoltaic cells sensitized by three-dimensional (3-D) methylammonium lead-halides ($MAPbX_3$, X: Br, I).[5] Since then, efficient perovskite solar cells with 3-D $MAPbX_3$ have been rapidly developed by Park's, Snaith's and Grätzel's groups.[6–9] In the case of the 3-D perovskites, their light-absorption and photoconductive properties are governed by the 3-D inorganic semiconducting framework.[10–13]

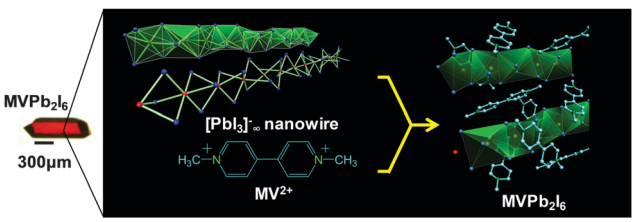

Fig. 1 Photograph of a single crystal of $MVPb_2I_6$ with back-side illumination and crystal structure.

On the other hand, the mentioned 1-D $MVPb_2I_6$ nanowire perovskite has intriguing optical and photoconductive properties, in which both the organic and inorganic components take part.[4,14,15]

As shown in Fig. 1, the 1-D $MVPb_2I_6$ perovskite is a unique nanowire material that consists of ultrathin face-sharing lead-iodide chains ($[PbI_3]^-_\infty$) with a diameter of *ca.* 0.5 nm and intervening organic electron-accepting MV^{2+} molecules.[16] $MVPb_2I_6$ shows a dark red crystal colour, although the inorganic nanowire and MV^{2+} have wide optical-gaps higher than 3.5 eV.[17–19] This dark-red coloration of $MVPb_2I_6$ results from the optical interfacial charge-transfer (ICT) transitions (so-called spatially indirect transitions) from the valence band of the lead-iodide nanowire to the unoccupied molecular orbitals of MV^{2+}, as shown in Fig. 2(a).[4,14,15] With the ICT transitions, $MVPb_2I_6$ shows a broad absorption band in the visible region in addition to a 1-D exciton

[a] *Research Center for Advanced Science and Technology (RCAST), The University of Tokyo, 4-6-1 Komaba, Meguro-ku, Tokyo 153-8904, Japan. E-mail: ufujisw@mail.ecc.u-tokyo.ac.jp*

[b] *Japan Science and Technology Agency (JST), Precursory Research for Embryonic Science and Technology (PRESTO), 4-1-8 Honcho Kawaguchi, Saitama 332-0012, Japan*

[c] *Department of Chemical System Engineering, School of Engineering, The University of Tokyo, 7-3-1, Hongo, Bunkyo-ku, Tokyo 113-8656, Japan*

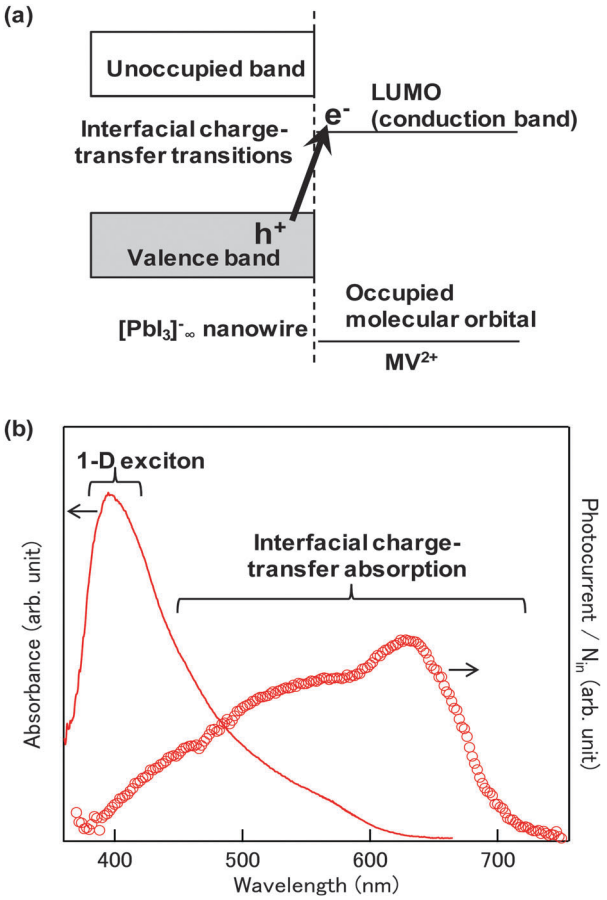

Fig. 2 (a) Schematic picture of staggered type-II band structure experimentally deduced for $MVPb_2I_6$ and (b) near UV-visible absorption spectrum of a cleaved crystal of $MVPb_2I_6$ (red curve) and the excitation spectrum of photocurrent divided by the incident photon number (N_{in}) for $MVPb_2I_6$ (red circles). The experimental data are reported in ref. 4 and 14.

absorption at 400 nm, as shown in Fig. 2(b). The ICT transitions induce photocurrent much more efficiently as compared to the 1-D exciton absorption.[4,14] In addition, the measurement of the anisotropy in the photoconductivity suggested ambipolar photocarrier transport, in which photogenerated electrons are transported three-dimensionally through the organic network and holes one-dimensionally in the nanowire.[4] Unfortunately, conclusive results concerning the staggered band structure (so-called type-II band alignment, see Fig. 2(a)) and electronic properties of photocarriers are not available yet. In this paper, we theoretically study the electronic band structure and photocarrier properties of $MVPb_2I_6$ by density functional theory (DFT) calculations.

Computational details

Both a periodic and a cluster approach have been employed in our research. Concerning the former, DFT calculations of the band structure of $MVPb_2I_6$ have been performed with the generalized gradient approximation as implemented in the VASP code[20,21] using the electron exchange–correlation functional proposed by Perdew–Burke–Ernzerhof (PBE).[22] The electron–ion interaction is described by the projector augmented wave method (PAW).[23,24] Also, still concerning the PAW potential, a $5d^{10}6s^26p^2$ valence electron potential was used for Pb atoms. The plane-wave basis set energy cut-off was 500 eV. For the structural optimization, a $2 \times 2 \times 2$ Γ-centered k-point sampling of the Brillouin Zone was used, while for the study of electronic properties denser meshes have been used (30 k-points). Due to the presence of heavy elements, relativistic effects are taken into account in the calculation of the electronic properties of $MVPb_2I_6$. Recent papers concerning Pb-based perovskite bulk systems have shown how the inclusion of spin–orbit coupling (SOC) effects becomes mandatory in order to obtain an improved description of the electronic structures.[12,13] In addition to the PBE functional, we also tested another GGA functionals,[25–27] as shall be described later. meta-GGA calculations require pseudopotentials including information on the kinetic energy density of the core-electrons; thus in this last case a slightly different set (compared with calculations at PBE + SOC level) of pseudopotentials were used. Negligible differences were found by the comparison of the results obtained with the two sets employed at the DFT level.

The experimental rhombohedral crystal structure reported by Tang *et al.*[16] ($R\bar{3}$, $Z = 3$) was used and kept frozen during the calculations. Since no hydrogen coordinates of MV^{2+} have been reported in their paper, the C–H bonds were optimized by DFT. Since $MVPb_2I_6$ includes heavy Pb and I atoms, spin–orbit couplings of all the atoms were taken into account. At the cluster level, DFT calculations of MV^{2+} and piperidinium ions (PD^+) were carried with the PBEPBE[22] functional and 6-31G+(d,p)[28,29] basis set using the Gaussian 09 software.[30] As reported by Matteo, for MV^{2+}, a slightly twisted structure about the inter-ring C–C bond is the most stable.[31] However, since MV^{2+} in $MVPb_2I_6$ has a planar form, our calculation was carried out with the restriction that the two methylpyridinium rings are coplanar. We confirmed that similar calculation results are obtained with other functionals such as B3LYP.[32,33]

Results and discussion

Fig. 3(a) and (b) show the PBE + SOC calculated band structure and density of states (DOS) of $MVPb_2I_6$, respectively. From these figures, we can see that the valence band mainly consists of the 5p (I) orbitals with a very minor contribution of the 6s (Pb) orbitals of the lead-iodide nanowires. Accordingly, the valence band is localized in the lead-iodide nanowires, as shown in Fig. 4(a). On the other hand, the conduction band in $MVPb_2I_6$ is located 0.82 eV above the valence band. The conduction band consists of 2p (C) and 2p (N) orbitals of the MV^{2+} molecules. As a consequence, in contrast to the valence band, the conduction band of $MVPb_2I_6$ is localized on the MV^{2+} molecules, as shown in Fig. 4(b). Therefore, the valence and conduction bands in $MVPb_2I_6$ are spatially separated in the inorganic and organic moieties, respectively. Thus, the PBE + SOC calculation reveals the experimentally reported staggered band alignment (Fig. 2(a)). However, the band gap (*ca.* 0.8 eV) of $MVPb_2I_6$ is quite

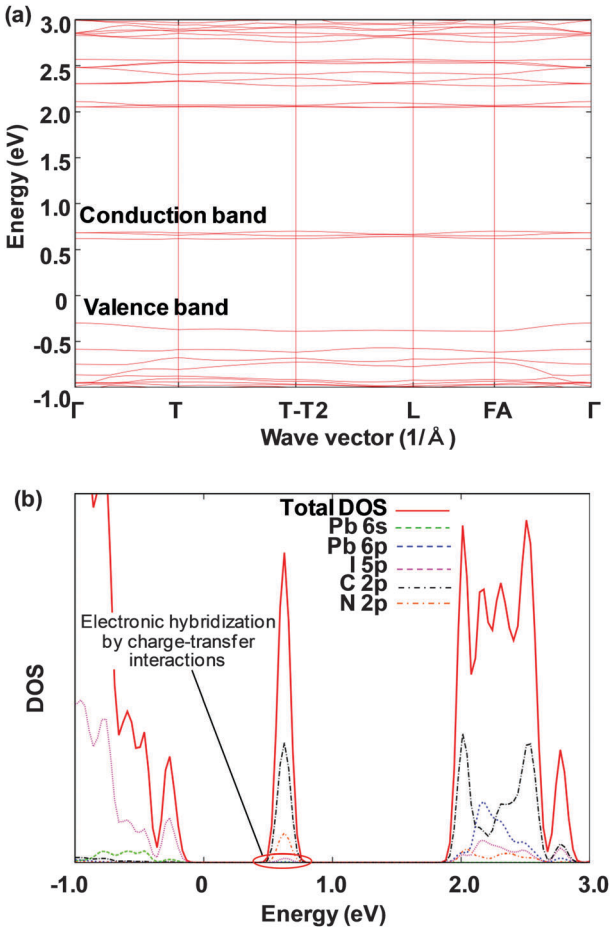

Fig. 3 (a) Band structure and (b) density of states (DOS) of $MVPb_2I_6$ calculated by DFT with the PBE functional including spin–orbit coupling effects.

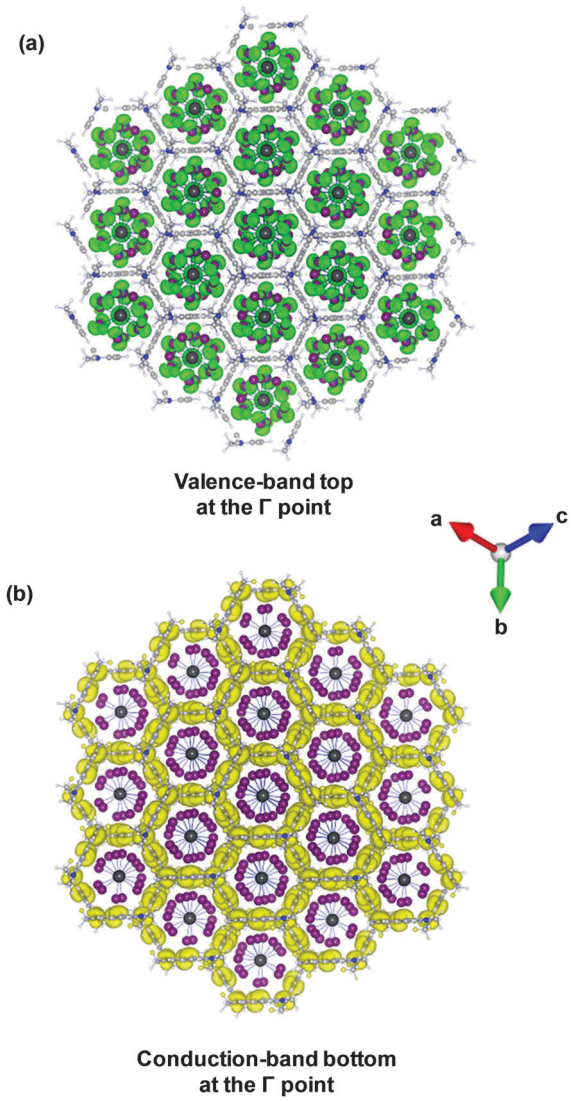

Fig. 4 Isosurface plots of electron-density distributions of (a) the top of the valence band (green isosurface) and (b) the bottom of the conduction band (yellow isosurface) in $MVPb_2I_6$ (isovalue = 0.0001). Large dark gray: lead; purple: iodine; small gray: carbon, blue: nitrogen, white: hydrogen atoms.

underestimated as compared to the absorption onset energy (2.15–2.16 eV)[4] of the ICT band. Such underestimation is considered to be a typical shortcoming of DFT calculations.[12,13] On the other hand, we found that the conduction band is weakly hybridized with the 5p orbitals of the I atoms. In addition, the DFT calculation suggests higher-energy unoccupied bands significantly delocalized on both the MV^{2+} molecules and lead-iodide nanowires. We examined the above-mentioned underestimation of the band gap using a meta-GGA functional, *i.e.* the RTPSS functional.[25] Using the RTPSS functional combined with SOC effects, the band gap is improved up to 1.55 eV on Γ as compared with that (0.82 eV) for PBE + SOC. However, the above-mentioned band-edge properties obtained with PBE + SOC are not altered in the RTPSS + SOC calculation. For this reason, we employ the calculation results obtained with PBE + SOC below.

We compare the electronic structure of $MVPb_2I_6$ with that of the 1-D $PDPbI_3$ perovskite reported by Azuma *et al.*[34] $PDPbI_3$ consists of similar lead-iodide nanowires to those in $MVPb_2I_6$ and piperidinium cations (PD^+) instead of MV^{2+}. For $PDPbI_3$, both the valence and conduction bands are localized in the lead-iodide nanowires, indicating a type-I band alignment. The atomic-orbital component of the valence band in $MVPb_2I_6$ almost agrees with that in $PDPbI_3$. Therefore, the difference in the electronic structure between $MVPb_2I_6$ (type-II) and $PDPbI_3$ (type-I) is considered to be due to the difference in electronic properties between MV^{2+} and PD^+.

Fig. 5 shows the DFT calculated energy-level diagram of the highest occupied molecular orbital (HOMO) and the lowest unoccupied molecular orbital (LUMO) of MV^{2+} and PD^+ in vacuum. The DFT calculations revealed that the LUMO of MV^{2+} is much lower in energy by 5.8 eV than that of PD^+. The deeper LUMO level is consistent with the electron-accepting property of MV^{2+}. We compare the electron-density distribution of the conduction-band bottom with the electronic distribution of the LUMO in MV^{2+}. As shown in Fig. 6, it can be seen that the conduction band of $MVPb_2I_6$ consists of the LUMO of MV^{2+}. Therefore, the difference in the band structure between $PDPbI_3$ (type-I) and $MVPb_2I_6$ (type-II) is attributed to the difference in the energy of the LUMO level between MV^{2+} and PD^+.

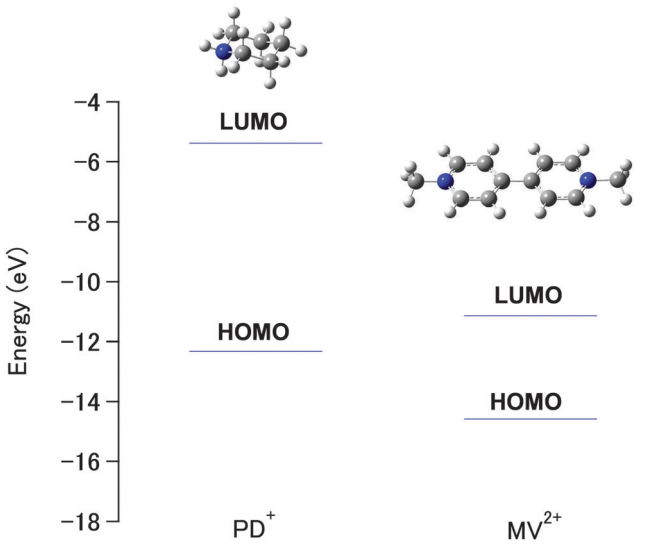

Fig. 5 Energy-level diagram of HOMO and LUMO of PD^+ and MV^{2+} calculated by DFT together with optimized structures of PD^+ and MV^{2+}. Gray: carbon; blue: nitrogen; white: hydrogen atoms.

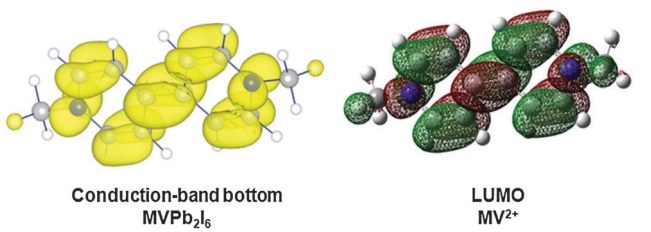

Fig. 6 Isosurface plots of electron-density distribution (yellow isosurface, isovalue = 0.0001) of the conduction-band bottom on MV^{2+} and electronic distribution (green and brown isosurfaces, isovalue = 0.02) of LUMO of MV^{2+}. Gray: carbon, blue: nitrogen, white: hydrogen atoms.

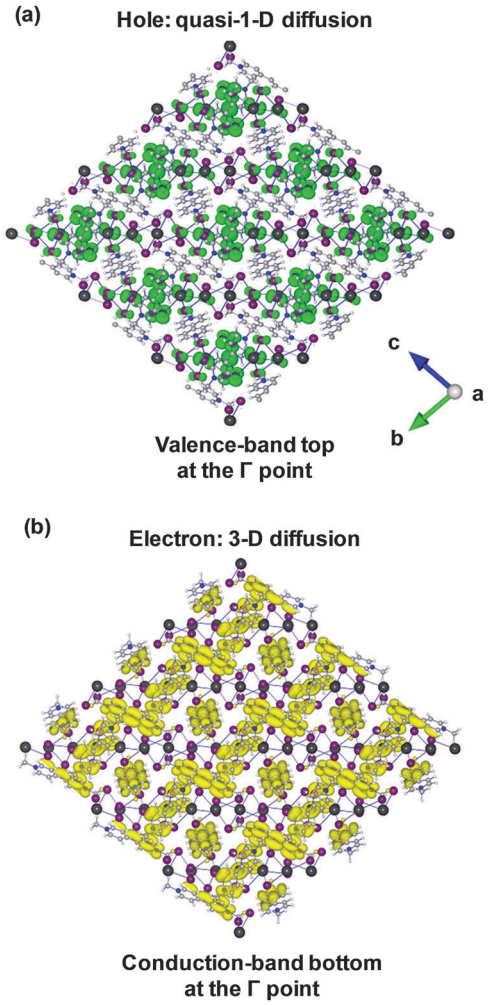

Fig. 7 Electron–density distributions of (a) the valence-band top (green isosurface, isovalue = 0.0001) and (b) conduction-band bottom (yellow isosurface, isovalue = 0.0001) viewed along the *a* axis.

As mentioned above, the conduction band localized on MV^{2+} is weakly hybridized with the 5p orbitals of I atoms in the lead-iodide nanowires, as shown in Fig. 3(b). Since the valence band is predominantly comprised of the 5p orbitals, the electronic hybridization is considered to result from weak charge-transfer interactions between the valence band located in the lead-iodide nanowires and LUMO of MV^{2+}. In the previous paper, we deduced the existence of the charge-transfer interactions between the lead-iodide nanowire and MV^{2+} from the vibrational structure measured by FT-IR.[15] The calculation result supports the deduction.

Here, we discuss the properties of the photocarrier transports in $MVPb_2I_6$ on the basis of the calculation results. At first, as shown in Fig. 3, the band widths of the conduction and valence bands are estimated to be less than *ca.* 0.3 eV. The narrow band widths imply the polaron formation of the photogenerated electrons and holes with the strong electron–lattice interactions in $MVPb_2I_6$.[4] Fujisawa *et al.* examined the electron–lattice interaction in $MVPb_2I_6$ from the analysis of the absorption tail of the ICT band using Urbach's equation ($A = A_0 \exp(\sigma\beta(E - E_0))$, σ: steepness constant).[4] The obtained steepness constant of 0.35 is quite small as compared to those (0.6–3) for other inorganic semiconductors and insulators.[35] This result indicates that the electron–lattice coupling in $MVPb_2I_6$ is quite strong. Thus, because of the narrow band widths of the conduction and valence bands and strong electron–lattice interaction, photogenerated electrons and holes are considered to relax to polarons. The polaron formation is consistent with the reported observation of the photoluminescence from spatially-separated polaron-pairs in $MVPb_2I_6$.[14]

The measurement of the anisotropy in the photoconductivity in $MVPb_2I_6$ indicated ambipolar photocarrier transport, in which photogenerated holes are transported one-dimensionally in the nanowire and electrons three-dimensionally through the organic network.[4] Fig. 7 shows the electron-density distributions of the valence and conduction bands viewed along the *a* axis. Since the inter-wire electronic coupling is quite weak as compared to the intra-wire one, as shown in Fig. 7(a), photogenerated hole-polarons are predominantly transported along the nanowire. On the other hand, photogenerated electron-polarons are considered to be transported by thermally-activated hopping through the 3-D organic network, since there are little electronic overlaps

between neighbouring molecules, as shown in Fig. 7(b). Therefore, the calculation result is consistent with the ambipolar transport.[4]

Conclusion

We theoretically verified the electronic band-structure of $MVPb_2I_6$ by the DFT calculations. The DFT calculation revealed the experimentally reported type-II band alignment, in which the conduction band is localized on the MV^{2+} molecules and the valence band in the lead-iodide nanowires. In addition, electronic hybridization between the conduction band on MV^{2+} and the valence band in the nanowires occurs by charge-transfer interactions. The narrow band widths (<0.3 eV) of the conduction and valence bands suggest the polaron formation of the photogenerated electrons and holes. Furthermore, the electronic distributions of the conduction and valence bands indicate the 3-D electron and 1-D hole transports, which are consistent with the reported experimental result.

Acknowledgements

This research was supported by the Precursory Research for Embryonic Science and Technology (PRESTO) program of the Japan Science and Technology Agency (JST). The author (G.G.) thanks Prof. Koichi Yamashita of the University of Tokyo for supporting the analysis of electronic properties of the material and for the always fruitful and stimulating scientific discussions.

Notes and references

1 T. Ishihara, in *Optical Properties of Low-Dimensional Materials*, ed. T. Ogawa and Y. Kanemitsu, World Scientific, Singapore, 1995, ch. 6.
2 G. C. Papavassiliou, *Prog. Solid State Chem.*, 1997, **25**, 125.
3 D. B. Mitzi, *Prog. Inorg. Chem.*, 1999, **48**, 121.
4 J. Fujisawa and N. Tajima, *Phys. Rev. B: Condens. Matter Mater. Phys.*, 2005, **72**, 125201.
5 A. Kojima, K. Teshima, Y. Shirai and T. Miyasaka, *J. Am. Chem. Soc.*, 2009, **131**, 6050.
6 H.-S. Kim, C.-R. Lee, J.-H. Im, K.-B. Lee, T. Moehl, A. Marchioro, S.-J. Moon, R. Humphry-Baker, J.-H. Yum, J. E. Moser, M. Grätzel and N.-G. Park, *Sci. Rep.*, 2012, **2**, 591.
7 M. M. Lee, J. Teuscher, T. Miyasaka, T. N. Murakami and H. J. Snaith, *Science*, 2012, **338**, 643.
8 J. Burschka, N. Pellet, S.-J. Moon, R. Humphry-Baker, P. Gao, M. K. Nazeeruddin and M. Grätzel, *Nature*, 2013, **499**, 316.
9 M. Liu, M. B. Johnston and H. J. Snaith, *Nature*, 2013, **501**, 395.
10 T. Umebayashi, K. Asai, T. Kondo and A. Nakao, *Phys. Rev. B: Condens. Matter Mater. Phys.*, 2003, **67**, 155405.
11 E. Mosconi, A. Amat, M. K. Nazeeruddin, M. Grätzel and F. D. Angelis, *J. Phys. Chem. C*, 2013, **117**, 13902.
12 J. Even, L. Pedesseau, J.-M. Jancu and C. Katan, *J. Phys. Chem. Lett.*, 2013, **4**, 2999.
13 G. Giorgi, J. Fujisawa, H. Segawa and K. Yamashita, *J. Phys. Chem. Lett.*, 2013, **4**, 4213.
14 J. Fujisawa and T. Ishihara, *Phys. Rev. B: Condens. Matter Mater. Phys.*, 2004, **70**, 113203.
15 J. Fujisawa, N. Tajima, K. Tamaki, M. Shimomura and T. Ishihara, *J. Phys. Chem. C*, 2007, **111**, 1146.
16 Z. Tang and A. Guloy, *J. Am. Chem. Soc.*, 1999, **121**, 452.
17 A. Nagami, K. Okamura and T. Ishihara, *Physica B*, 1996, **227**, 346.
18 T. Fukumoto, M. Hirasawa and T. Ishihara, *J. Lumin.*, 2000, **87–89**, 497.
19 M. Mohammad, *J. Org. Chem.*, 1987, **52**, 2779.
20 G. Kresse and J. Furthmüller, *Comput. Mater. Sci.*, 1996, **6**, 15.
21 G. Kresse and J. Furthmüller, *Phys. Rev. B: Condens. Matter Mater. Phys.*, 1996, **54**, 11169.
22 J. P. Perdew, K. Burke and M. Ernzerhof, *Phys. Rev. Lett.*, 1996, **77**, 3865.
23 P. E. Blöchl, *Phys. Rev. B: Condens. Matter Mater. Phys.*, 1994, **50**, 17953.
24 G. Kresse and D. Joubert, *Phys. Rev. B: Condens. Matter Mater. Phys.*, 1999, **59**, 1758.
25 J. Sun, M. Marsman, G. I. Csonka, A. Ruzsinszky, P. Hao, Y.-S. Kim, G. Kresse and J. P. Perdew, *Phys. Rev. B: Condens. Matter Mater. Phys.*, 2011, **84**, 035117.
26 A. D. Becke and E. R. Johnson, *J. Chem. Phys.*, 2006, **124**, 221101.
27 F. Tran and P. Blaha, *Phys. Rev. Lett.*, 2009, **102**, 226401.
28 R. Ditchfield, W. Hehre and J. Pople, *J. Chem. Phys.*, 1971, **54**, 724.
29 W. Hehre, R. Ditchfield and J. Pople, *J. Chem. Phys.*, 1972, **56**, 2257.
30 M. J. Frisch, *et al.*, *Gaussian 09, Revision D.01*, Gaussian, Inc., Wallingford, CT, 2009.
31 A. di Matteo, *Chem. Phys. Lett.*, 2007, **439**, 190–198.
32 A. D. Becke, *J. Chem. Phys.*, 1993, **98**, 5648.
33 C. Lee, W. Yang and R. G. Parr, *Phys. Rev. B: Condens. Matter Mater. Phys.*, 1988, **37**, 785.
34 J. Azuma, K. Tanaka, M. Kamada and K. Kan'no, *J. Phys. Soc. Jpn.*, 2002, **71**, 2730.
35 M. Ueta, H. Kanzaki, K. Kobayashi, Y. Toyozawa and E. Hanamura, *Excitonic Processes in Solids*, Springer-Verlag, Tokyo, 1984.